

# AUTOMATIC ESTIMATION OF ICE BOTTOM SURFACES FROM RADAR IMAGERY

Mingze Xu<sup>†</sup>      David J. Crandall<sup>†</sup>      Geoffrey C. Fox<sup>†</sup>      John D. Paden<sup>\*</sup>

<sup>†</sup> School of Informatics and Computing, Indiana University, Bloomington, IN USA

<sup>\*</sup> Center for Remote Sensing of Ice Sheets, University of Kansas, Lawrence, KS USA

## ABSTRACT

Ground-penetrating radar on planes and satellites now makes it practical to collect 3D observations of the subsurface structure of the polar ice sheets, providing crucial data for understanding and tracking global climate change. But converting these noisy readings into useful observations is generally done by hand, which is impractical at a continental scale. In this paper, we propose a computer vision-based technique for extracting 3D ice-bottom surfaces by viewing the task as an inference problem on a probabilistic graphical model. We first generate a seed surface subject to a set of constraints, and then incorporate additional sources of evidence to refine it via discrete energy minimization. We evaluate the performance of the tracking algorithm on 7 topographic sequences (each with over 3000 radar images) collected from the Canadian Arctic Archipelago with respect to human-labeled ground truth.

**Index Terms**— Glaciology, Radar tomography, 3D reconstruction, Graphical models

## 1. INTRODUCTION

Scientists increasingly use visual observations of the world in their work: astronomers collect telescope images at unprecedented scale [1], biologists image live cells [2, 3], sociologists record social interactions [4], ecologists collect large-scale remote sensing data [5], etc. Although progress in technology has made *collecting* this imagery affordable, actually *analyzing* it is often done by hand. But with recent progress in computer vision, automated techniques may soon work well enough to remove this bottleneck, letting scientists analyze visual data more thoroughly, quickly, and economically.

As a particular example, glaciologists need large-scale data about the polar ice sheets and how they are changing over time in order to understand and predict the effects of melting glaciers. Aerial ground-penetrating radar systems have been developed that can fly over an ice sheet and collect evidence about its subsurface structure. The raw radar return data is typically mapped into 2D radar echogram images which are easier for people to interpret, and then manually labeled for important semantic properties (ice thickness and structure, bedrock topography, etc.) in a slow, labor-intensive process [6, 7, 8, 9]. Some recent work has shown promis-

ing results on the specific problem of layer-finding in 2D echograms [10, 11, 12], although the accuracy is still far below that of a trained human annotator. The echograms are usually quite noisy and complex, requiring experience and intuition that is difficult to encode in an algorithm. Using echograms as input data also inherently limits the analysis to the ice structure immediately under the radar’s flight path.

In this paper we take an alternative approach, using additional data collected by the radar in order to actually estimate the 3D structure of the ice sheet, including a large area on either side, instead of simply tracing 2D cross-sections (Figure 1). In particular, the Multichannel Coherent Radar Depth Sounder (MCoRDS) instrument [13] uses three transmit beams (left, nadir, right) to collect data from below the airplane and to either side (for a total swath width of about 3km). Although an expert may be able to use intuition and experience to produce a reasonable estimate of the 3D terrain from this data, the amount of weak evidence that must be considered at once is overwhelming. As with structure-from-motion in images [14], this gives automatic algorithms an advantage: while humans are better at using intuition to estimate from weak evidence, algorithms can consider a large, heterogeneous set of evidence to make better overall decisions.

We formulate the problem as one of discrete energy minimization in order to combine weak evidence into a 3D reconstruction of the bottom of the ice sheet. We first estimate layer boundaries to generate a seed surface, and then incorporate additional sources of evidence, such as ice masks, surface digital elevation models, and optional feedback from humans to refine it. We investigate the performance of the algorithm using ground truth from humans, showing that our technique significantly outperforms several strong baselines.

## 2. RELATED WORK

Detecting boundaries between material layers in noisy radar images is important for glaciology. Semi-automated and automated methods have been introduced for identifying features of subsurface imaging. For example, in echograms from Mars, Freeman et al. [6] find layer boundaries by applying band-pass filters and thresholds to find linear subsurface structures, while Ferro and Bruzzone [15] identify subterranean features using iterative region-growing. For the

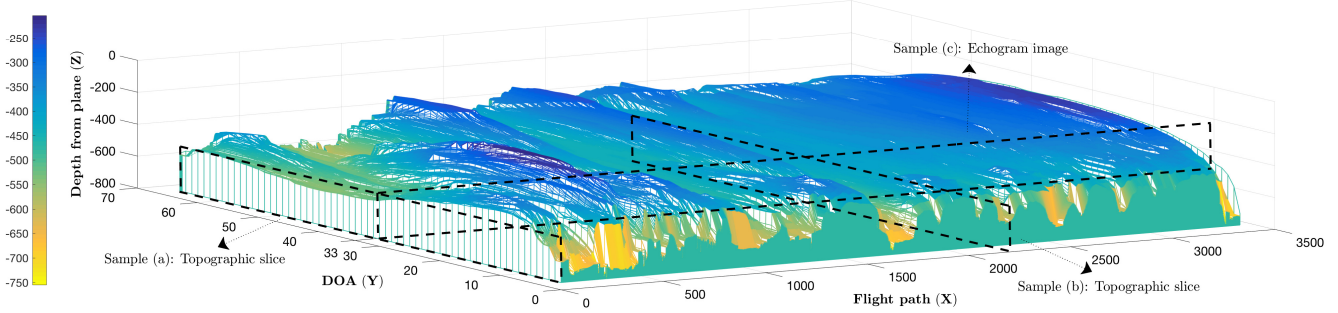


**Fig. 1.** Illustration of our task. Radar flies along the X-axis, collecting noisy evidence about the ice surface distance and depth immediately below it. This yields a 2D echogram (Sample (c)), with depth on one axis and flight path on the other, and prior work has used these echograms to estimate 2D ice structure but only along the flight path. Our approach also includes (very noisy) evidence from either side of the radar, yielding a sequence of 2D topographic slices (e.g. Sample (a) and (b)). Each slice is represented in polar coordinates, where Y- and Z-axis denote the direction of arrival of radar waves and the distance from each voxel to plane, respectively. We combine this noisy evidence with prior information to produce 3D ice reconstructions.

specific case of ice, Crandall et al. [10] detect the ice-air and ice-bottom layers in echograms along the flight path by combining a pretrained template model for the vertical profile of each layer and a smoothness prior in a probabilistic graphical model. Lee et al. [11] present a more accurate technique that uses Gibbs sampling from a joint distribution over all possible layers. Carrer and Bruzzone [12] reduce computational complexity with a divide-and-conquer strategy. In contrast to the above work which all infers 2D cross-sections, we attempt to reconstruct 3D subsurface features and are not aware of other work that does this. We pose this as an inference problem on a Markov Random Field similar to that proposed for vision problems (e.g. stereo [16]), except that we have a large set of images and wish to produce a 3D surface, whereas they perform inference on a single 2D image at a time.

### 3. METHODOLOGY

As the radar system flies over ice, it collects a sequence of topographic slices  $I = \{I_1, \dots, I_l\}$  that characterizes the returned radar signals (Figure 1). Each slice  $I_i$  is a 2D radar image that describes a distribution of scattered energy in polar coordinates (with dimensions  $\phi \times \rho$ ) at a discrete position  $i$  of the aircraft along its flight path. Given such a topographic sequence of dimension  $l \times \phi \times \rho$ , we wish to infer the 3D ice-bottom surface. We parameterize the surface as a sequence of slices  $S = \{S_1, \dots, S_l\}$  and  $S_i = \{s_{i,1}, \dots, s_{i,\phi}\}$ , where  $s_{i,j}$  denotes the row coordinate of the boundary of the ice-bottom for column  $j$  of slice  $i$ , and  $s_{i,j} \in [1, \rho]$  since the ice-bottom layer can occur anywhere within a column.

#### 3.1. A graphical model for surface extraction

Because radar is so noisy, our goal is to find a surface that not only fits the observed data well but that is also smooth and satisfies other prior knowledge. We formulate this as an inference problem on a Markov Random Field. In particular,

we look for a surface that minimizes an energy function,

$$E(S|I) = \sum_{i=1}^l \sum_{j=1}^{\phi} \psi_1(s_{i,j}|I) + \quad (1)$$

$$\sum_{i=1}^l \sum_{j=1}^{\phi} \sum_{i' \in \pm 1} \sum_{j' \in \pm 1} \psi_2(s_{i,j}, s_{i+i', j+j'}) \quad (2)$$

where  $\psi_1(\cdot)$  defines a unary cost function which measures how well a given labeling agrees with the observed image in  $I$ , and  $\psi_2(\cdot, \cdot)$  defines a pairwise interaction potential on the labeling which encourages the surface to be continuous and smooth. Note that each column of each slice contributes one term to the unary part of the energy function, while the pairwise terms are a summation over the four neighbors of a column (two columns on either side within the same slice, and two slices within the same column in neighboring slices).

**Unary term.** Our unary term  $\psi_1(\cdot)$  consists of three parts,

$$\psi_1(\cdot) = \psi^{temp}(\cdot) + \psi^{air}(\cdot) + \psi^{bin}(\cdot). \quad (3)$$

First, similar to [10], we define a template model  $T$  of fixed size  $1 \times t$  (we use  $t = 11$  pixels) for the vertical profile of the ice-bottom surface in each slice. For each pixel  $p$  in the template, we estimate a mean  $\mu_p$  and a variance  $\sigma_p$  on greyscale intensity assuming that the template is centered at the location of the ice-bottom surface, suggesting a template energy,

$$\psi^{temp}(s_{i,j}|I) = \sum_{p \in T} (I(s_{i,j} + p) - \mu_p)^2 / \sigma_p. \quad (4)$$

We learn the parameters of this model with a small set of labeled training data.

Second, to capture the fact that the ice-bottom surface should always be below the ice-air surface by a non-trivial

|                          | Error |             | Precision |          |
|--------------------------|-------|-------------|-----------|----------|
|                          | Mean  | Median Mean | 1 pixel   | 5 pixels |
| (a) Ice-bottom surfaces: |       |             |           |          |
| Crandall [10]            | 101.6 | 95.9        | 0.2%      | 2.5%     |
| Lee [11]                 | 35.6  | 30.5        | 3.6%      | 29.9%    |
| Ours with DV             | 13.3  | 13.4        | 20.2%     | 58.3%    |
| Ours with TRW            | 11.9  | 12.2        | 35.9%     | 63.9%    |
| (b) Bedrock layers:      |       |             |           |          |
| Crandall [10]            | 75.3  | 42.6        | 0.5%      | 21.5%    |
| Lee [11]                 | 47.6  | 36.6        | 2.2%      | 20.5%    |
| Ours with TRW            | 4.1   | 4.2         | 28.8%     | 81.4%    |

**Table 1.** Error in terms of the mean and median mean absolute column-wise difference compared to ground truth, in pixels. Precision is the percentage of correct labeled pixels.

margin, we add a cost to penalize intersecting surfaces,

$$\psi^{air}(s_{ij}) = \begin{cases} +\infty & s_{i,j} - a_{i,j} < 0 \\ 0 & s_{i,j} - a_{i,j} > \tau \\ \tau - |s_{i,j} - a_{i,j}| & \text{otherwise,} \end{cases} \quad (5)$$

with  $a_{i,j}$  the label of the air-ice boundary of slice  $i$ , column  $j$ .

Finally, we incorporate an additional weak source of evidence produced by the radar system. The *bottom bin* gives a constraint on a *single* column in each slice, specifying a single coordinate  $(j, b_i)$  that the true surface boundary must be below. Despite how weak this evidence is, it helps to distinguish between the ice-air and ice-bottom surface boundary in practice. Formally, we formulate this cost function as,

$$\psi^{bin}(s_{i,j}) = \begin{cases} +\infty & s_{i,j} < b_i \\ 0 & \text{otherwise.} \end{cases} \quad (6)$$

**Pairwise term.** The ice-bottom surface is encouraged to be smooth across both adjacent columns and adjacent slices,

$$\psi_2(s, \hat{s}) = \begin{cases} -\beta_j \ln \mathcal{N}(s - \hat{s}; 0, \hat{\sigma}) & |s - \hat{s}| < \alpha \\ +\infty & \text{otherwise,} \end{cases} \quad (7)$$

where  $\hat{s}$  denotes the labeling of an adjacent pixel of  $(i, j)$ , and parameters  $\alpha$  and  $\hat{\sigma}$  are learned from labeled training data. Parameter  $\beta_j$  models smoothness on a per-slice basis, which is helpful if some slices are known to be noisier than others (or set to a constant if this information is not known). This term models the similarity of the labeling of two adjacent pixels by a zero-mean Gaussian that is truncated to zero outside a fixed interval  $\alpha$ . Since all parameters in the energy function are considered penalties, we transform the Gaussian probability to a quadratic function by using a negative logarithm.

Our energy function introduces several important improvements over that of Crandall et al. [10] and Lee et al. [11]. First, while their model gives all pairs of adjacent pixels the

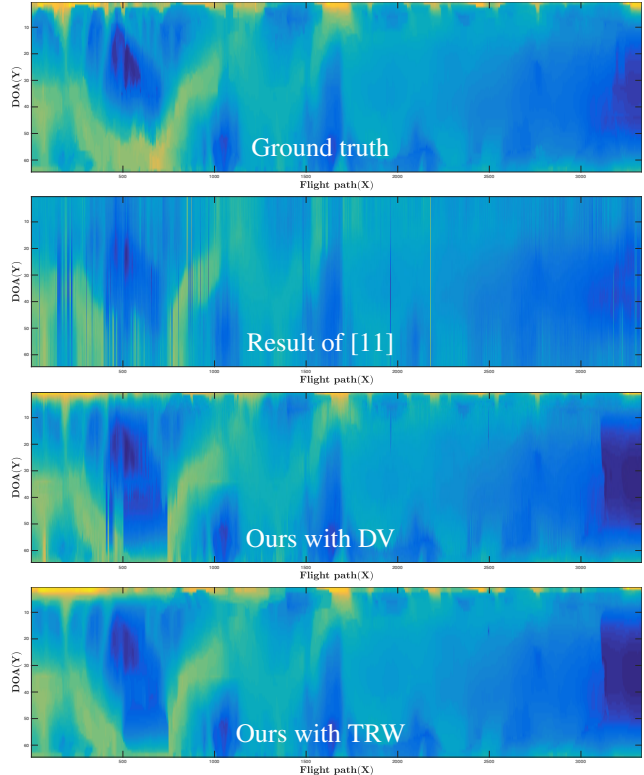


**Fig. 2.** Results of the ice-bottom surface extracting on a sample dataset. The color represents the depth from plane (Z).

same pairwise weight ( $\beta$ ), we have observed that layers in different slices usually have particular shapes, such as straight lines and parabolas, depending on the local ice topography. By using a dynamic weight  $\beta_j$ , we can roughly control the shape of the layer and adjust how smooth two adjacent pixels should be. More importantly, those techniques consider a single image at a time, which could cause discontinuities in the ice reconstruction. We correct this by defining pairwise terms along both the intra- and inter-slice dimensions.

### 3.2. Statistical inference

The minimization of equation (1) can be formulated as discrete energy minimization on a first-order Markov Random Field (MRF) [17]. Given the large size of this MRF, we use Sequential Tree-reweighted Message Passing (TRW) [18], which breaks the MRF into several monotonic chains, and perform belief propagation (BP) on each chain. TRW only passes messages within each of these chains, rather than to all four directions (like Loopy BP [19]). Benefiting from this, TRW converges faster and requires half as much memory as traditional message passing methods. We assign a row-major order for pixels in the graph and define the monotonic chains based on this order. In each iteration, TRW first passes messages in increasing order, and then back in decreasing order. We pre-define a maximum number of iterations to be the same as the width of each slice,  $\phi$ , which allows evidence from one

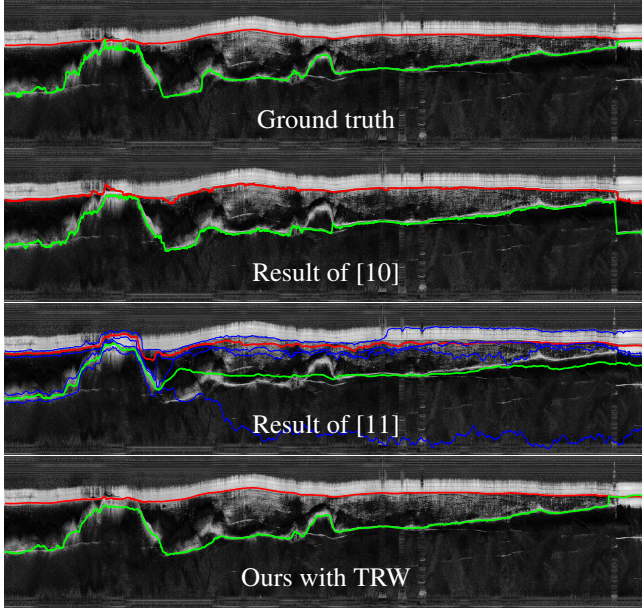


**Fig. 3.** Results of the bedrock layer finding on a sample echogram. In each image, the upper (red) boundary is the ice-air layer, and the lower (green) boundary is the ice-bottom layer. The ice-air layer in our result is from the radar.

side of the slice to reach the other. When message passing is finished, we assign a label to each pixel in row-major order: for pixel  $(i, j)$ , we choose the label  $s_{i,j}$  that minimizes  $M(s_{i,j}) + \psi_1(s_{i,j}) + \psi_2(s_{i,j}, s_{i,j-1}) + \psi_2(s_{i,j}, s_{i-1,j})$ , where  $M(s_{i,j})$  is the summation of messages from four adjacent neighbors.

The usual implementation of TRW has time complexity  $O(l\phi\rho^2)$  for each loop. To speed this up, we use linear-time generalized distance transforms [16], yielding a total running time of  $O(l\phi\rho L)$  where  $L$  is the number of iterations. This is possible because of our pairwise potentials are log-Gaussian.

#### 4. EXPERIMENTS

We tested our surface extraction algorithm on the basal topography of the Canadian Arctic Archipelago (CAA) ice caps, collected by the Multichannel Coherent Radar Depth Sounder (MCoRDS) instrument [13]. We used a total of 7 topographic sequences, each with over 3000 radar images which corresponds to about 50km of flight data per sequence. For these images, we also have the associated ice-air surface ground truth, a subset (excluded from the testing data) of which we used to learn the parameters of the template model and the weights of the binary costs.

We then ran inference on each topographic sequence and measured the accuracy by comparing our estimated surfaces to the ground truth, which was produced by human annotators. However, these labels are not always accurate at the pixel-level, since the radar images are often full of noise, and some boundaries simply cannot be tracked precisely even by

experts. To relax the effect of inaccuracies in ground truth, we consider a label to be correct when it is within a few pixels. We evaluated with three summary statistics: mean deviation, median mean deviation, and the percentage of correct labeled pixels over the whole surface (Table 1(a)). The mean error is about 11.9 pixels and the median-of-means error is about 12.2 pixels. The percentage of correct pixels is 35.9%, or about 63.9% within 5 pixels, which we consider the more meaningful statistic given noise in the ground truth.

To give some context, we compare our results with three baselines. Since no existing methods solve the 3D reconstruction problem that we consider here, we adapted three methods from 2D layer finding to the 3D case. Crandall et al. [10] use a fixed weight for the pairwise conditional probabilities in the Viterbi algorithm, which cannot automatically adjust the shape of the layer in each image slice. Lee et al. [11] generate better results by using Markov-Chain Monte Carlo (MCMC). However, neither of these approaches considers constraints between adjacent slices. We introduce Dynamic Viterbi (DV) as an additional baseline that incorporates a dynamic weight for the pairwise term, but it still lacks the ability to smooth the whole surface in 3D. As shown in Table 1(a) and Figure 2, our technique performs significantly better than any of these baselines on 3D surface reconstruction. We also used our technique to estimate layers in 2D echograms, so that we could compare directly to the published source code of [10, 11] (i.e. using our approach to solve the problem they were designed for). Figure 3 and Table 1(b) present results, showing a significant improvement over these baselines also.

Similar to [10, 11], additional evidence can be easily added into our energy function. For instance, ground truth data (e.g. ice masks) may be available for some particular slices, and human operators can also provide feedback by marking true surface boundaries for a set of pixels. Either of these can be implemented by putting additional terms into the unary term defined in equation (3).

#### 5. CONCLUSION

To the best of our knowledge, this paper is the first to propose an automated approach to reconstruct 3D ice features using graphical models. We showed our technique can effectively estimate ice-bottom surfaces from noisy radar observations. This technique also demonstrated its accuracy and efficiency in producing bedrock layers on radar echograms against the state-of-the-art.

#### 6. ACKNOWLEDGEMENTS

This work was supported in part by the National Science Foundation (DIBBs 1443054, CAREER IIS-1253549), and used the Romeo cluster, supported by Indiana University and NSF RaPyDLI 1439007. We acknowledge the use of data from CREsis with support from the University of Kansas and Operation IceBridge (NNX16AH54G).



## 7. REFERENCES

- [1] Alexander Szalay and Jim Gray, “The world-wide telescope,” *Science*, vol. 293, no. 5537, pp. 2037–2040, 2001.
- [2] Jyoti K Jaiswal, Hedi Mattoussi, J Matthew Mauro, and Sanford M Simon, “Long-term multiple color imaging of live cells using quantum dot bioconjugates,” *Nature Biotechnology*, vol. 21, no. 1, pp. 47–51, 2003.
- [3] David J Stephens and Victoria J Allan, “Light microscopy techniques for live cell imaging,” *Science*, vol. 300, no. 5616, pp. 82–86, 2003.
- [4] Claus Wedekind and Manfred Milinski, “Cooperation through image scoring in humans,” *Science*, vol. 288, no. 5467, pp. 850–852, 2000.
- [5] Jonathan Bamber, Jennifer Griggs, Ruud Hurkmans, Julian Dowdeswell, Prasad Gogineni, Ian Howat, Jeremie Mougnot, John Paden, Steven Palmer, Eric Rignot, et al., “A new bed elevation dataset for Greenland,” *The Cryosphere*, vol. 7, no. 2, pp. 499–510, 2013.
- [6] Greg J Freeman, Alan C Bovik, and John W Holt, “Automated detection of near surface martian ice layers in orbital radar data,” in *Southwest Symposium on Image Analysis & Interpretation (SSIAI)*, 2010, pp. 117–120.
- [7] Ana-Maria Ilisei, Adamo Ferro, and Lorenzo Bruzzone, “A technique for the automatic estimation of ice thickness and bedrock properties from radar sounder data acquired at Antarctica,” in *International Geoscience and Remote Sensing Symposium (IGARSS)*, 2012, pp. 4457–4460.
- [8] Adamo Ferro and Lorenzo Bruzzone, “Automatic extraction and analysis of ice layering in radar sounder data,” *IEEE Transactions on Geoscience and Remote Sensing*, vol. 51, no. 3, pp. 1622–1634, 2013.
- [9] Jerome E Mitchell, David J Crandall, Geoffrey C Fox, and John D Paden, “A semi-automatic approach for estimating near surface internal layers from snow radar imagery,” in *International Geoscience and Remote Sensing Symposium (IGARSS)*, 2013, pp. 4110–4113.
- [10] David J Crandall, Geoffrey C Fox, and John D Paden, “Layer-finding in radar echograms using probabilistic graphical models,” in *International Conference on Pattern Recognition (ICPR)*, 2012, pp. 1530–1533.
- [11] Stefan Lee, Jerome Mitchell, David J Crandall, and Geoffrey C Fox, “Estimating bedrock and surface layer boundaries and confidence intervals in ice sheet radar imagery using MCMC,” in *International Conference on Image Processing (ICIP)*, 2014, pp. 111–115.
- [12] Leonardo Carrer and Lorenzo Bruzzone, “Automatic enhancement and detection of layering in radar sounder data based on a local scale hidden Markov model and the Viterbi algorithm,” *IEEE Transactions on Geoscience and Remote Sensing*, vol. 55, no. 2, pp. 962–977, 2017.
- [13] Fernando Rodriguez-Morales, Sivaprasad Gogineni, Carlton J Leuschen, John D Paden, Jilu Li, Cameron C Lewis, Benjamin Panzer, Daniel Gomez-Garcia Alvestegui, Aqsa Patel, Kyle Byers, et al., “Advanced multifrequency radar instrumentation for polar research,” *IEEE Transactions on Geoscience and Remote Sensing*, vol. 52, no. 5, pp. 2824–2842, 2014.
- [14] David J Crandall, Andrew Owens, Noah Snavely, and Daniel P Huttenlocher, “SfM with MRFs: Discrete-continuous optimization for large-scale structure from motion,” *IEEE Transactions on Pattern Analysis and Machine Intelligence*, vol. 35, no. 12, pp. 2841–2853, 2013.
- [15] Adamo Ferro and Lorenzo Bruzzone, “A novel approach to the automatic detection of subsurface features in planetary radar sounder signals,” in *IEEE International Geoscience and Remote Sensing Symposium (IGARSS)*, 2011, pp. 1071–1074.
- [16] Pedro F Felzenszwalb and Daniel P Huttenlocher, “Efficient belief propagation for early vision,” *International Journal of Computer Vision*, vol. 70, no. 1, pp. 41–54, 2006.
- [17] Daphne Koller and Nir Friedman, *Probabilistic graphical models: principles and techniques*, MIT Press, 2009.
- [18] Vladimir Kolmogorov, “Convergent tree-reweighted message passing for energy minimization,” *Transactions on Pattern Analysis and Machine Intelligence*, vol. 28, no. 10, pp. 1568–1583, 2006.
- [19] Kevin P Murphy, Yair Weiss, and Michael I Jordan, “Loopy belief propagation for approximate inference: An empirical study,” in *Proceedings of the Fifteenth Conference on Uncertainty in Artificial Intelligence*, 1999, pp. 467–475.